Performance of Variable Flow Rates for Photovoltaic-Thermal Collectors and the Determination of Optimal Flow Rates

T. Dembeck-Kerekes[a], Jamie P. Fine[b], J. Friedman[b], S.B. Dworkin[b], J. J. McArthur[a*]

[a]Architectural Science, Ryerson University, 350 Victoria Street, Toronto, Canada

[b]Mechanical and Industrial Engineering, Ryerson University, 350 Victoria Street, Toronto, Canada

*Corresponding Author.

Email Address: jjmcarthur@ryerson.ca

Abstract

A quasi-steady state model has been developed to asses of the potential of variable flow strategies to improve the overall thermal efficiency of Photovoltaic-thermal (PVT) collectors. An adaption of the Duffie-Beckman method is used to simulate the PVT, in which the overall loss coefficient and heat removal factor are updated at each timestep in response to changes in flow rate and ambient conditions. A novel calculation engine was also developed to simulate a building heating loop connected to the solar loop via a counterflow heat exchanger that calculates the steady-state conditions for the system at each timestep. The results from PVT simulation are in good agreement with test data obtained from the solar simulator – environmental chamber facility at Concordia University. Further validation for the overall system was carried out via a parallel simulation run in TRNSYS and the model-predicted annual solar heat gains were within 3.6%. The results of the investigation show that a variable flow rate strategy has significant potential to improve thermal efficiency. This benefit was found to be dependent on ambient and process loop conditions, and most effective for systems with greater difference between heating process supply and return temperatures.

Keywords: Photovoltaic-thermal; Solar Thermal; Flow Rate Optimization; variable flow

1 Introduction

1.1 Research Motivation

Photovoltaic-thermal (PVT) collectors can produce electricity and heat at the same time, and as such they provide an intriguing alternative to both traditional flat plate thermal and photovoltaic (PV) collectors. If the thermal energy captured can be applied as useful energy, the overall system efficiency of PVT is often higher than that of a combination of PV and solar thermal panels occupying the same area. Quantifying and improving the performance of PVTs have been significant topics of ongoing research resulting in advances in panel construction, system operation techniques, and new applications for PVT systems (Al-Waeli, et al., 2017; Kumar, et al., 2015; Sathe & Dhoble, 2017). This paper contributes significantly to this discourse by investigating a variable flow control strategy to optimize useful energy generation.

Many studies in the literature have found that varying the liquid flow rate through the collector can have an appreciable effect on system performance. A study by Al-Waeli et al. (2018) found that increasing the flow rate of liquid through a PVT collector could reduce heat loss from the panel and improve system performance. Their study focused on incorporating nanoparticles into the fluid, rather than focusing on flow rate optimization. Additional studies by Al-Waeli et al. studied the incorporation of nanoparticles and phase change materials with PVT panels in great detail, including aspects related to grid-connected systems (Al-Waeli, et al., 2018), neural networks (Al-Waeli, et al., 2018), experimental studies (Al-Waeli, et al., 2017), and computational fluid dynamics (CFD) modelling (H, et al., 2017). Another study by Yazdanifard et al. (2016) investigated the effect of operating a solar collector in the turbulent and laminar flow regimes. Their study found that operating a panel with a flow rate in the turbulent regime typically produced higher overall system efficiency compared to laminar regime operation, but with lower fluid outlet temperatures. Their study focused primarily on the design of the solar collector, rather than flow rate optimization. Finally, a study by Nasrin et al. (2018) investigated the effect of varying fluid flow rate in a PVT collector, with a focus on cooling the PV cells to improve electrical efficiency at high irradiation levels. This study found that increasing the fluid flow rate will increase both the thermal and electrical efficiency of the system, and that this diminishes at high levels. The focus of their study was on overall collector performance analysis, rather than varying the flow rate to achieve a controlled fluid outlet temperature. While these articles do not specifically focus on outlet temperature control by varying the flow rate, they show the appreciable effect that flow rate can have on the performance of a PVT system and the widespread interest in characterizing this effect.

Varying the collector fluid flow rate allows for the outlet temperature of the fluid from the panel to be controlled for different operating conditions, which can be ideal for supplying building systems such as domestic hot water and space heating. Studies on flow optimization have been performed for systems incorporating thermal storage. Nhut and Park (2013) performed an analysis of evacuated tube collectors to provide domestic hot water heating through a thermal storage tank in South Korea. They performed simulations to determine the optimal flow coefficient to control flow rate based on the outlet temperature from the collectors and the tank temperature, which provided the largest net energy balance between useful solar heat gains and pump electrical consumption. The coefficient was used to examine the effects of varying thermal tank volumes, initial temperatures, and total collector area on the system. They concluded that the optimal flow strategy yielded a 1.54% increase in useful solar heat gain, and reduced pump power by 65.61%. Badescu (2008) undertook a similar study with much more positive results. A model was developed consisting of flat plate solar thermal collectors that deliver heat to a thermal storage tank in one of two configurations: direct fluid transfer to the tank and with internal heat exchanger. The optimal flow rate was identified using the Pontryaghin principle, and it was found that nearly twice as much thermal energy was added to the thermal storage tank using the optimal flow strategy as opposed to a constant flow rate. Finally, Hollands and Brunger (1992) modelled a system with a counterflow heat exchanger between the flat plate solar array and the thermal storage tank. They concluded that an optimal flow rate exists for the loops on both sides of the heat exchanger. The same optimization methods used for systems without the heat exchanger between the tank and solar array can be used, and that the optimal flow rate is the same if an adjustment factor is applied to the collector area.

Some studies considered variable flow to produce a constant output temperature. For example, Calise et al. (2012) performed a study of a solar tri-generation system using PVTs in which the flow rate through the PVTs was varied to achieve the desired output temperature. The output temperature target was changed in winter and summer according to the intended use of the solar output heat. However, achievement of the target temperature is highly dependent on the climatic conditions, the input temperature requirement of the downstream process, and the size of the solar array. In light of their study, it is important to note that under conditions where constant target temperature is not possible or practical the variation in flow rate can still be optimized to maximize solar heat gains for the particular conditions. This minimizes the need for additional top-up energy to boost the output temperature to the requirement of the target process, and increases the percentage of energy loads supplied by solar.

Other studies tested the effects of different constant flow rates on annual thermal energy gains. Kalogiru (2001) used TRNSYS to simulate a PVT collector for domestic hot water heating in Cyprus, using six different constant flow rates. It was found that useful energy gain was strongly affected by the flow rate. It increased to a peak, and then decreased steadily to zero thereafter as the flow rate was increased. Similarly, Nualboonrueng et al. (2013) simulated a PVT collector for domestic hot water production in Bangkok using TRNSYS. Their results showed a similar trend, where the different flow rate values had a significant impact on annual useful energy gain by the for a given system; while a *particular* constant flow rate performs better than others aggregated over the course of a year, that flow rate may not be optimal at any given *moment* within that year.

This paper expands upon these observations by investigating variable flow rate strategies to optimize solar thermal efficiency in systems without thermal storage. The modelling technique used in this paper for PVTs is capable of assessing the potential of flowrate changes at each timestep to improve performance at variable current ambient conditions and building loads. The PVT model is integrated into a closed loop system that includes a heating process loop and heat exchange via a counterflow heat exchanger.

1.2 Solar Panel Model Selection

Existing literature was reviewed to select the most appropriate model for accurate PVT performance prediction under varying flow rates. The primary parameters considered were the level of accuracy, adaptability to different operating conditions on the scale of individual time steps, and the level of complexity of the model and associated computational cost. Zondag et al. (2001) performed an investigation into the effectiveness of 1D, 2D, and 3D models for predicting yields of PVT collector systems, examining the differences between dynamic and steady state modelling. The steady state model determines the thermal conditions when the panel has reached thermal equilibrium, ignoring both the heat capacity of components and their temperature change over time, while the dynamic model considers the temperatures of the components to be transient and time dependant. They found that when comparing simple steady-state 1D models to complex 3D dynamic models, the average efficiency over the course of a day differed by only 0.2% on a clear day and by 0.0% on a day with highly fluctuating solar radiation. The differences between these two models occurred at the beginning and end of the day due to thermal mass effects considered only in the dynamic model. The solar gains between the two models when simulating only the first three hours of sunlight were 0.8% for the clear day, and 2.3% for the highly fluctuating solar radiation day. Meanwhile the computational cost for these models varied significantly; the time required to simulate one hour varied from 0.05 seconds for the 1D steady-state model to 2.5 hours for the 3D dynamic model. Weighing the minimal discrepancy between models against the substantial increase in computational time, they concluded that simple, steady state models are appropriate for predicting daily system performance for a given application using hourly time steps.

Several simple steady state models have been used to characterize collector performance and predicting solar energy gains over extended periods. The methodology presented by Duffie and Beckman using the Hottel-Whillier-Bliss equation, provides the basis for the simple steady state model (Duffie & Beckman, 1991):

$$Q_u = A_c F_r (I(\tau\alpha) - U_l(T_i - T_a)) \tag{1}$$

where Q_u is the useful heat gain, A_c is the collector aperture area, F_r is the heat removal factor, I is the solar irradiance, $(\tau\alpha)$ is the optical efficiency, U_l is the overall loss coefficient, T_i is the solar fluid inlet temperature, and T_a is the ambient temperature. The optical efficiency and overall loss coefficient constitute the performance characterization of the collector, and are typically considered constant for a particular collector fluid flow rate and ambient wind speed.

Many studies in the literature use the Hottel-Whillier-Bliss equation, or a modified version thereof to predict the performance of a PVT system. Vokas et al. (2005) calculated the average collector performance as a function of the panel reduced temperature. This characterization was linear with reduced temperature, and was applied using the F-chart method to compare the energy generation potential of a conventional thermal collector to a PVT collector for solar heating and cooling in three cities in Greece. In another study, Bencheikh El-Hocine et al. (2015) investigated the performance of a PVT collector with a galvanized iron absorber plate, using inlet and outlet temperatures and useful thermal energy as performance indicators. A one-dimensional model using the Hottel-Whillier-Bliss equation was created to simulate the panel, and the model was validated using experimental results. Anderson et al. (2008) created a model based on a modified Hottel-Whillier-Bliss equation to investigate the impacts of different panel physical parameters on thermal efficiency. Absorber materials and conductivity, absorber-PV bond conduction, riser tube width, transmittance-absorption product, and insulation thickness were varied and the thermal efficiency was plotted versus reduced temperature. The Duffie-Beckman method was also modified to simulate different amounts of PV coverage over the absorber plate. Finally, Dubey and Tiwari (2008) used Duffie-Beckman as a base for a quasi-steady state model to evaluate a new PVT design for standalone hot water heating in New Delhi, including a thermal storage tank. PV modules encased in glass on both sides to replace the glazing cover of a flat plate collector and three different fractions of PV coverage for their collector were investigated. The model developed incorporated a variable transmittance-absorptance product for the collector, which accounted for the changing amount of PV cells shading the absorber plate, with a static heat removal factor and overall loss coefficient for the collectors. The results of their model were validated against experimental data, and their predictions for output temperature had a correlation coefficient above 0.999 when compared to their test data. Together, these papers demonstrate the flexibility and application of the Hottel-Whillier-Bliss equation as used in combined with the Duffie-Beckman method to accurately model PVT collector performance.

There are limitations to how the Duffie-Beckman method and Hottel-Whillier-Bliss are typically used in simulation models. The Hottel-Whillier-Bliss equation is often used to characterize the performance of a collector on a reduced temperature graph, where the y-axis is the thermal efficiency of the collector (η_c), and the x-axis is the difference in temperature between the collector fluid inlet and the ambient air, divided by the solar irradiance ($(T_i-T_a)/G$). The efficiency is then characterized by the optical efficiency $(\tau\alpha)$ multiplied by the heat removal factor (F_r) as the y-intercept. The slope of the line can be considered linear, in which case it is equal to $-U_lF_r$. In reality, the overall loss coefficient increases with increasing reduced temperature due to the fourth order relationship with radiative heat loss. This causes the efficiency line to be non-linear, and an additional temperature dependence value for the overall loss coefficient to reduced temperature is often included to account for it. Assuming these values are constant, the efficiency can be determined from the ambient temperature, solar irradiance, and fluid inlet temperature at any given point. As noted by Touafek et al. (2011), this characterization is critical as it provides a standard for solar thermal panel experimental testing and performance characterization. However, the performance characterization using a reduced temperature graph is accurate only so long as three variables remain constant: flow rate, wind speed, and the ambient reference temperature. Of these, the latter two are less significant, although their effects become more pronounced as the reduced temperature increases.

The modelling approach presented in this study addresses these limitations by reassessing those parameters each time there is a change in ambient conditions, flow rate, or fluid inlet temperature. This adaptation is significant as it permits the Duffie-Beckman calculation method for solar thermal panels to be used in simulations with variable flow control strategies, addressing the lack of research investigating novel control strategies as well as improving simulation accuracy from its typical adoption at high reduced temperatures.

2 Model Development

2.1 PVT Collector

The PVT collector used in this model is a flat plate thermal collector with PV laminate attached on top of the absorber plate. Cover glass is included above the PV layer to reduce heat loss, and is offset from the PV layer by a sealed air gap. The fluid pipes used for thermal energy extraction are bonded underneath the absorber plate and run parallel to each other lengthwise along the collector. The pipe material, inner diameter, cross-section, spacing, and bonding resistance are all inputs to this analysis.

A modified version of the Hottel-Whillier-Bliss equation is used to obtain the instantaneous efficiency of the collector based upon operating conditions. In this modified version, heat removal factors and overall heat loss coefficient are updated at each time step in order to investigate dynamic flow controls.

Since the loss coefficient increases as the temperature difference between the collector and ambient increases, a non-linear relationship exists between thermal efficiency and reduced temperature. This is primarily due to the fourth-order relationship between radiative heat loss from the absorber and the temperature difference between the absorber and ambient environment. The effect of temperature dependence on heat loss is particularly relevant for the variable flow strategy being proposed, since reducing the panel flow rate will cause the panel temperature to increase and the non-linearity of radiative heat loss to temperature relationship is more pronounced at higher temperatures. As mentioned in Section 1.2, the overall heat loss coefficient and heat removal factor are also heavily dependent on flow rate, and to a lesser extent wind speed and ambient temperature, therefore these performance parameters must be updated at each timestep to account for the changes in those critical input conditions.

The model assumes that incoming solar radiation is first reduced by optical losses through the cover glass, with the remainder being absorbed by the absorber plate as heat. The optical efficiency of the collector $(\tau\alpha)$ is given by the relationship shown in Eq. (2):

$$(\tau\alpha) = \tau_c \alpha_p \tag{2}$$

where τ_c is the transmittance of the cover, and α_p is overall absorption coefficient of the absorbing surface. If the absorbing surface is non-uniform, such as when the absorber plate is only partially covered by PV, an area-weighted average for absorption should be used (Dubey & Tiwari, 2008).

A fraction of the solar energy reaching the absorber plate is then converted into electricity by the PV cells, and the amount of electrical energy generation is determined using the PV cell efficiency. This cell efficiency is dependent on the PV cell temperature, and is defined by the characteristics of the cells (Dubey, et al., 2013):

$$\eta_e = \eta_o (1 - \beta_o (T_{PV} - T_{ref})) \tag{3}$$

where η_e is the electrical efficiency, η_o is the nominal cell electrical efficiency, T_{ref} is the reference temperature, T_{PV} is the cell temperature, and β_o is the temperature dependence coefficient of the cell. For hybrid panel analysis, the PV cell temperature is typically set equal to the average absorber plate temperature, which allows for model simplification (Chow, 2003).

An iterative calculation method is used to determine the collector thermal and electrical output using the system conditions at each time step, which is the method presented by Duffie and Beckman (1991). Absorbed heat is either transferred to the cooling fluid as useful thermal energy, or lost to the environment. To determine the portion of that energy that is useful, the Hottel-Whillier-Bliss equation is used and has been modified to include PV generation (Duffie & Beckman, 1991):

$$Q_u = A_c F_r (I\left((\tau\alpha) - \tau_c \eta_e\right) - U_l (T_i - T_a)) \tag{4}$$

As suggested by Zondag et al. (2001) and Anderson et al. (2008), the collector efficiency factor (F') should be modified to include the thermal resistance of the bond between the solar laminate and the absorber plate, therefore, the heat transfer coefficient of the bond between the absorber plate and PV laminate (h_{PV}) was added:

$$F' = \frac{\frac{1}{U_l}}{W\left(\frac{1}{U_l(d + (W - d)F) + \frac{1}{C_b} + \frac{1}{\pi d h_{fi}} + \frac{1}{W h_{PV}}}\right)} \tag{5}$$

where W is the distance between riser pipes, d is the outer diameter of the riser pipes, C_b is the conductance of the riser to absorber plate bond, and h_{fi} is the heat transfer coefficient between the fluid and the interior of the pipes.

Since a PV laminate has been added to the absorber plate, the M term has been modified to include its thermal conductance in addition to the absorber plate (Vokas, et al., 2005):

$$M = \sqrt{\frac{U_T}{k_{ab}\delta_{ab} + k_{PV}\delta_{PV}}} \tag{6}$$

where k denotes conductivity and δ thickness, and the subscripts ab and PV represent the absorber plate and PV laminate, respectively.

The useful heat (Q_u) is calculated using Eq. (4), using initial conditions for the cover and absorber plate temperatures to obtain the heat removal factor (F_r) and overall loss coefficient (U_l). It is important to note that the initial conditions are only used as a starting point for the iterative process, and that the final result is not dependant on this selection. An iterative loop is created wherein the useful heat (Q_u) is then used to update the plate temperature value using Eq. (7), which as derived based upon Eq. (4). The new plate temperature value is used to recalculate the cover temperature and associated heat loss coefficients. This process is repeated until two consecutive calculated values for the plate temperature are within a designated convergence tolerance.

$$T_p = T_i + \frac{\frac{Q_u}{A_c}}{F_R U_l}(1 - F_R) \tag{7}$$

The useful heat gain determined by Eq. (4) is dependent on η_e because the solar radiation that is converted into electricity by the PV is not available to become heat, and η_e is in turn a function of T_p as shown in Eq. (3). Since these variables are interdependent, an iterative process is used wherein after T_p is updated, a new electrical efficiency is determined using Eq. (3), and the useful heat gain is re-evaluated using those values with Eq. (4) until the updated plate temperature converges within a specified tolerance.

Once all iterative loops have converged, the collector efficiency can be determined as the useful heat collected divided by the amount of solar energy falling on the collector (Duffie & Beckman, 1991):

$$\eta_c = \frac{Q_u}{A_c I} \tag{8}$$

where η_c is the collector thermal efficiency, and I is the solar insulation.

2.2 *Building Heating with Counterflow Heat Exchanger*

The potential of variable flow was evaluated in a system where heat from the solar loop is directly transferred to the building heating loop through a counterflow heat exchanger with an assumed 70% heat transfer effectiveness. The heating loop is assumed to have constant supply and return values and the flow rate for the loop (mfr_b) is therefore simply a function of the building heating demand for a given timestep. A mixing loop is included to reduce the temperature exiting the heat exchanger if it exceeds the supply temperature. An auxiliary heater is included after the mixing valve. A system layout can be seen in Figure 1.

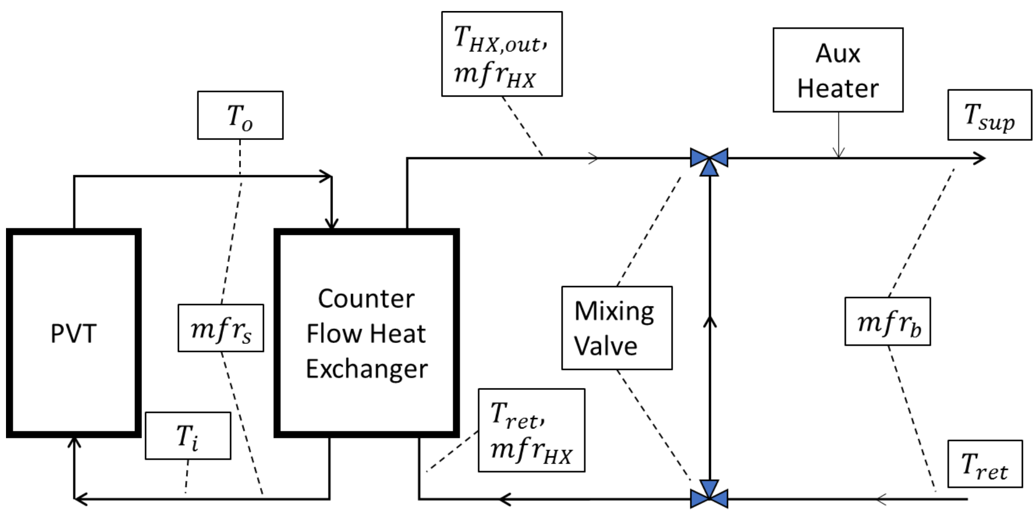

Figure 1: System Layout with Flow and Temperature Variable Labels

The performance of the counterflow heat exchanger in this model is based upon the minimum stream heat capacity method (TRNSYS, 2018). The maximum rate of heat transfer through the heat exchanger is the minimum of the heat capacity rates of the two streams, shown for the solar loop and heating loop side of the HX loop in Eqs. (9) and (10) respectively, and denoted in further calculations as C_{min}.

$$C_s = mfr_s Cp_s \tag{9}$$

$$C_{HX} = mfr_{HX} Cp_{HX} \tag{10}$$

where C is heat capacity rate of the stream, mfr is the mass flow rate of the stream, Cp is the heat capacity of the fluid in the stream, and the subscripts s and HX denote the solar and building heating streams passing through the heat exchanger respectively.

The maximum possible heat transfer rate occurs when the outlet temperature of the fluid stream with the lowest heat capacity rate reaches the inlet temperature of the second stream. Therefore, the actual rate of heat transfer for the solar and heating loops is (TRNSYS, 2018):

$$\dot{Q} = C_{min}(T_o - T_{ret})\epsilon_{HX} \tag{11}$$

where $\dot{Q}$ is the rate of heat transfer between the loops, T_o is the outlet temperature of the solar array, and T_{ret} is the return temperature of the heating loop, and ϵ_{HX} is the selected effectiveness of the heat exchanger.

The output temperature of the heat exchanger re-entering the solar collectors is found by taking an energy balance of the fluid stream through the heat exchanger, and is thus:

$$T_i = T_o + \frac{\dot{Q}}{C_s} \tag{12}$$

where T_i is the inlet temperature of the solar array.

Similarly, by again using an energy balance of the fluid steam through the heat exchanger, the building heating loop output temperature from the heat exchanger can be determined:

$$T_{HX,out} = T_{ret} + \frac{\dot{Q}}{C_{HX}} \tag{13}$$

where $T_{HX,out}$ is the outlet temperature from the heat exchanger on the heating loop side.

Some of aspects of the system are interdependent, and thus an iterative process is used to solve it. The flow chart presented in Figure 2 illustrates the solution process.

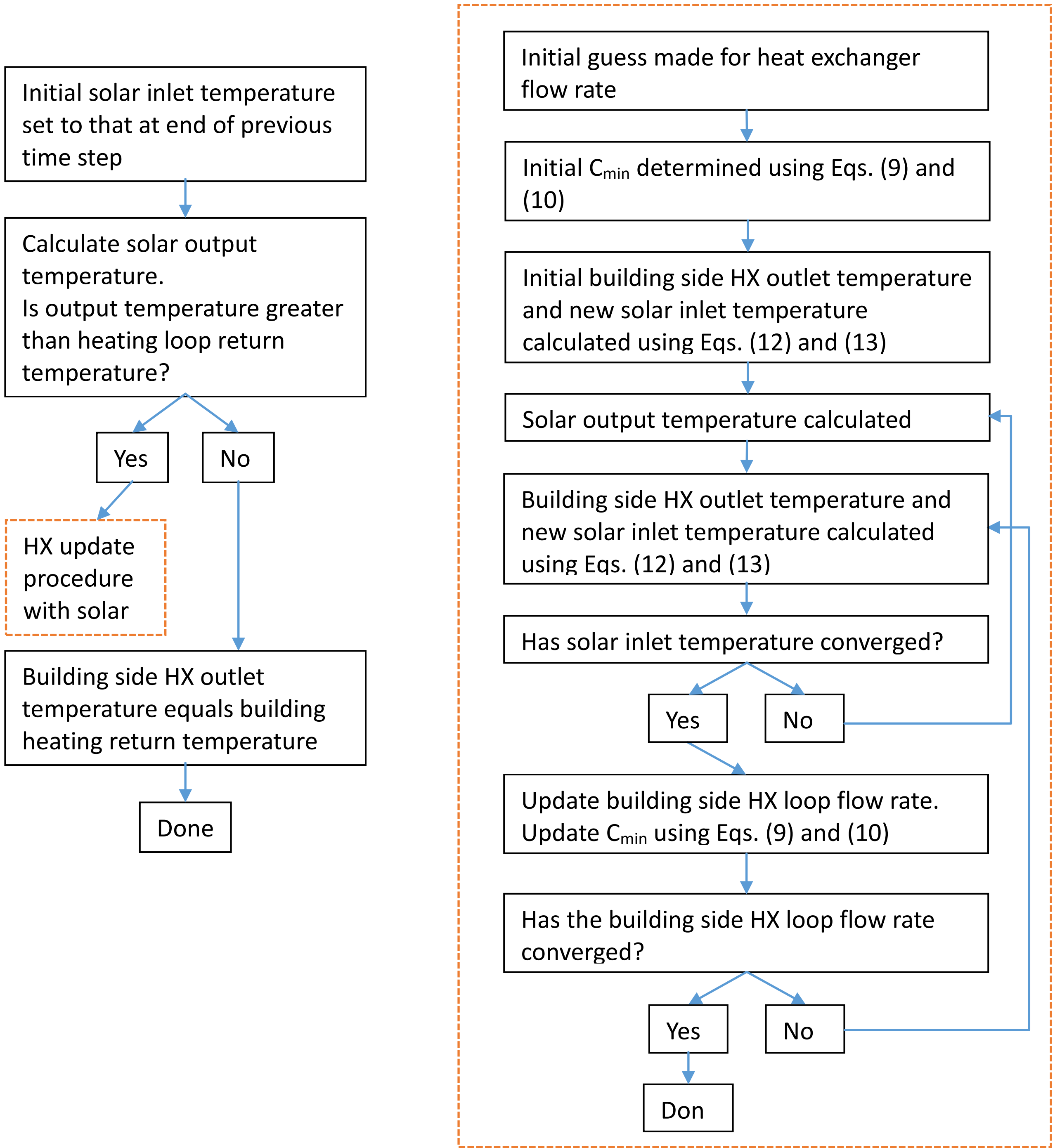

Figure 2: Heat Exchanger Steady State Solution Process

3 Model Validation

3.1 PVT Panel Performance Model

Validation for the PVT model was done using experimental test results using the Volther Powertherm shown in Figure 3. The testing was done at Concordia University in October 2017 in the Solar Simulator – Environmental Chamber laboratory. Temperature measurements of the fluid and air were taken using resistance temperature detectors with a resolution of 0.01°C. The apparatus was mounted perpendicular to the incoming radiation from the solar lamps as seen in Figure 4. Solar radiation was measured by scanning the grid before the apparatus was mounted in the space that it would occupy, using a pyranometer. Small fluctuations in the readings were averaged across the grid to obtain the measured value.

Figure 3: Volther Powertherm PVT Panel

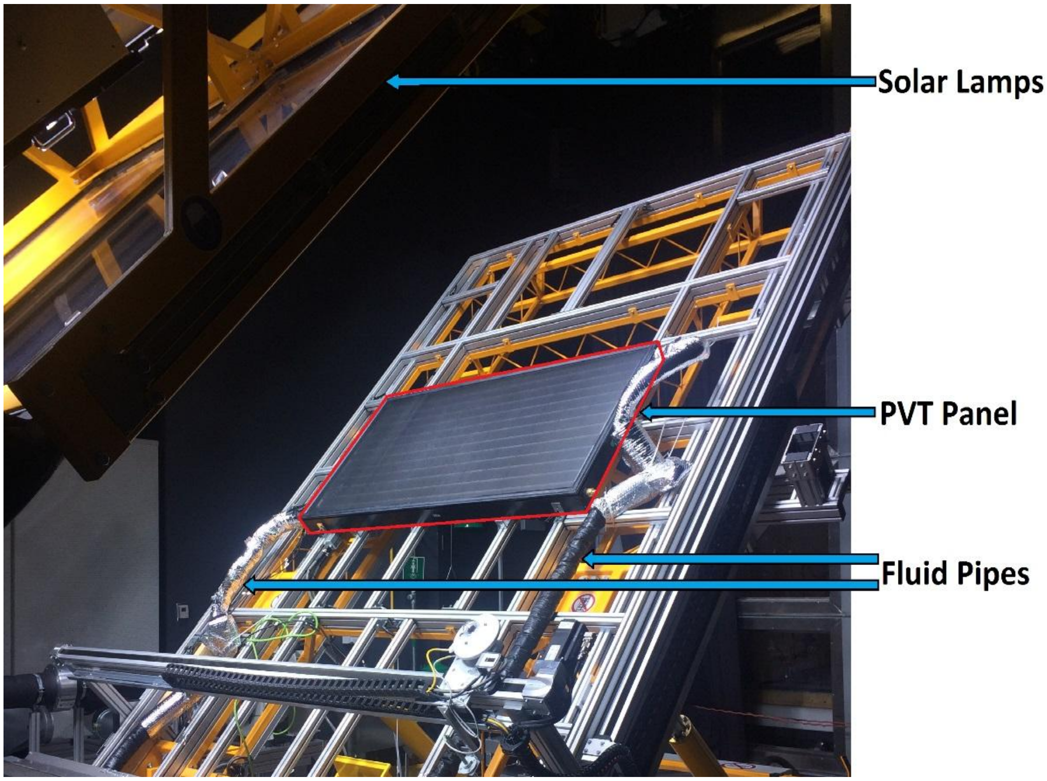

Figure 4: Experimental Set-Up in the Solar Simulation Lab at Concordia University

In all, 35 tests were conducted in which the ambient conditions, flow rate, and fluid inlet temperature were held constant until the fluid outlet temperature reached steady state. Steady state in these tests was assumed to have been attained when the outlet fluid temperature changed by no more than 0.01°C over a period of two minutes. The tests were organized into four groups wherein the wind speed, flow rate, and ambient temperature were held constant while the solar irradiance and fluid inlet temperatures were varied. The data from each group could therefore be used to create a reduced temperature graph characterizing the collector's performance at the designated wind speed and flow rate. A summary of the test conditions and results can be seen in Inputs for the custom model were taken from Volther Powertherm product datasheets and are summarized in

Table 2. Note that the PV Bond Conductance $\varepsilon_{c,}$ Plate Emissivity $\varepsilon_{p,}$ and PV Conductivity k_{PV} were not published for this panel and were assigned commonly-used values from the literature (specifically , , and , respectively). The measured values for electrical generation during the tests were used as inputs for the simulation. A sensitivity analysis was conducted for the following crucial parameters that were not given in the product specifications: the bond conductivity between the absorber plate and PV, side and bottom losses, and transmittance-absorption product. Figure 5 shows the measured versus simulated results for the sensitivity analysis under Case A conditions, where it was found that PV Bond Conductance h_{PV} = 30 W/m^{2}K, Side-Bottom Loss Coefficient U_{SB} = 1.5 W/m^{2}K, and the transmittance-absorptance product $(\tau\alpha)$ = 0.72 had the closest correlation with the measured results. Figures 6, 7, and 8 show the comparative results for Cases B-D using those values.

Table 1. Temperatures were recorded every five seconds, and final values are the average of the recordings during the two-minute steady-state period. It is important to note that the selected insolation values were based upon the limitations of the testing facility, which can only produce spectrally accurate and uniform solar radiation between ~900 W/m^2 and ~1300 W/m^2.

Inputs for the custom model were taken from Volther Powertherm product datasheets and are summarized in

Table 2. Note that the PV Bond Conductance $\varepsilon_{c,}$ Plate Emissivity $\varepsilon_{p,}$ and PV Conductivity k_{PV} were not published for this panel and were assigned commonly-used values from the literature (specifically (Anderson, et al., 2008), (Vokas, et al., 2005), and (Krauter, 2006), respectively). The measured values for electrical generation during the tests were used as inputs for the simulation. A sensitivity analysis was conducted for the following crucial parameters that were not given in the product specifications: the bond conductivity between the absorber plate and PV, side and bottom losses, and transmittance-absorption product. Figure 5 shows the measured versus simulated results for the sensitivity analysis under Case A conditions, where it was found that PV Bond Conductance h_{PV} = 30 W/m^{2}K, Side-Bottom Loss Coefficient U_{SB} = 1.5 W/m^{2}K, and the transmittance-absorptance product $(\tau\alpha)$ = 0.72 had the closest correlation with the measured results. Figures 6, 7, and 8 show the comparative results for Cases B-D using those values.

Table 1: Test Case Parameters and Results

Test Number	T_{in} [°C]	T_{out} [°C]	T_a [°C]	I [W/m^2]	Thermal Power [W]	Electrical Power [W]
Case A: mass flow rate = 103 kg/hr, wind speed = 2.6 m/s, PVT On						
2	21.90	27.64	22.29	1062	683.7	145.0
6	13.57	19.86	22.29	1062	751.0	149.5
8	40.37	44.84	22.36	1062	532.3	135.9
10	59.23	62.46	23.08	1062	391.6	134.8
12	13.16	18.34	20.79	899	618.0	132.4
14	21.49	26.20	21.36	899	567.1	124.3
32	58.99	61.48	22.48	899	299.4	108.1
18	40.77	46.44	22.43	1301	675.2	163.8
21	22.21	29.12	22.97	1301	828.2	174.9
22	13.87	21.23	23.03	1301	883.8	180.2
33	59.46	63.98	23.66	1301	540.7	151.9
Case B: mass flow rate = 43 kg/hr, wind speed = 2.6 m/s, PVT On						
4	21.69	34.62	22.55	1062	647.6	143.2
7	13.24	26.61	22.32	1062	699.9	149.0
9	39.70	49.68	22.94	1062	522.6	135.2
11	57.99	65.25	23.31	1062	396.8	126.4
Case C: mass flow rate = 103 kg/hr, wind speed = 5.8 m/s, PVT On						
24	12.84	18.84	22.50	1062	716.7	151.0
27	21.74	27.19	22.16	1062	647.9	146.8
31	58.75	60.76	22.73	899	242.6	108.9
35	72.55	73.33	22.27	899	93.5	103.8
Case D: mass flow rate = 103 kg/hr, wind speed = 2.6 m/s, PVT Off						
34	13.90	21.12	23.02	1062	860.8	0.0
1	22.18	28.79	22.20	1062	786.6	0.0
3	21.98	28.38	22.15	1062	760.8	0.0
29	40.64	45.87	22.52	1062	625.6	0.0
13	13.34	19.26	21.01	899	709.9	0.0
15	21.67	27.07	21.16	899	650.0	0.0
16	40.30	44.59	21.41	899	511.4	0.0
19	40.96	47.60	22.79	1301	791.2	0.0
20	22.45	30.39	22.99	1301	952.0	0.0
23	14.06	22.46	23.54	1301	1004.5	0.0

The mean absolute error for Cases A-D are 0.44%, 0.51%, 1.17%, and 2.25% respectively. Because the assumed collector characteristics were calibrated to Case A, increases in error from it to the other test cases can be attributed to the changes in the test parameters. In Case C, the wind speed was increased, indicating that the empirical formula used to determine the heat loss coefficient from the cover to ambient due to wind was slightly inaccurate. Case D turned off the PV generation and had the largest error from Case A. The model assumes that all incoming solar radiation is first converted into electricity by the PV, and the remainder is available to become heat. It is likely that this assumption is an oversimplification and the source of error in this case.

Table 2: Model Inputs for Volther Powertherm Physical Parameters

Variable	Variable	Value	Unit
Collector Area	Ac	1.4	m^2
Cover Emissivity	ε_c	0.88*	-
Plate Emissivity	ε_p	0.95*	-
Pipe-Fluid Heat Transfer Coefficient	h_{fi}	300	W/m^2*K
Plate-Pipe Bond Conductivity	C_b	100	W/m*K
Pipe Diameter	d	0.008	m
Pipe Spacing	W	0.11	m
Absorber Conductivity	k_{abs}	400	W/m*K
PV Conductivity	k_{PV}	130*	W/m*K
Absorber Thickness	δ_{abs}	0.00012	m
PV Thickness	δ_{PV}	0.04	m
Collector Tilt	β	45	°
Nominal Electrical Efficiency*	η_e	12.44	%
Nominal Thermal Efficiency* (Zero Loss Collector Efficiency)	η_t	0.486	-

**Efficiency values per manufacturer documentation in standard test conditions* (Solimpeks, 2016)

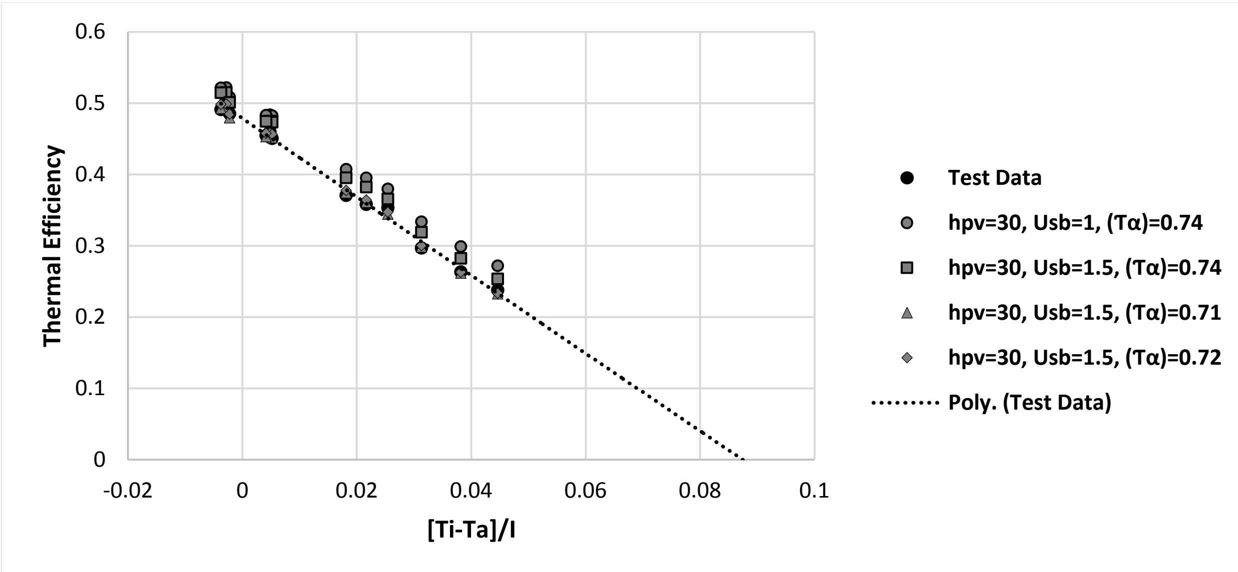

Figure 5: Case A (mass flow rate = 103 kg/hr, wind speed= 2.6 m/s, PVT On) - Reduced Temperature Thermal Efficiency, Measured vs. Simulated Results Using Different Side/Bottom Loss Coefficients and Optical Efficiencies

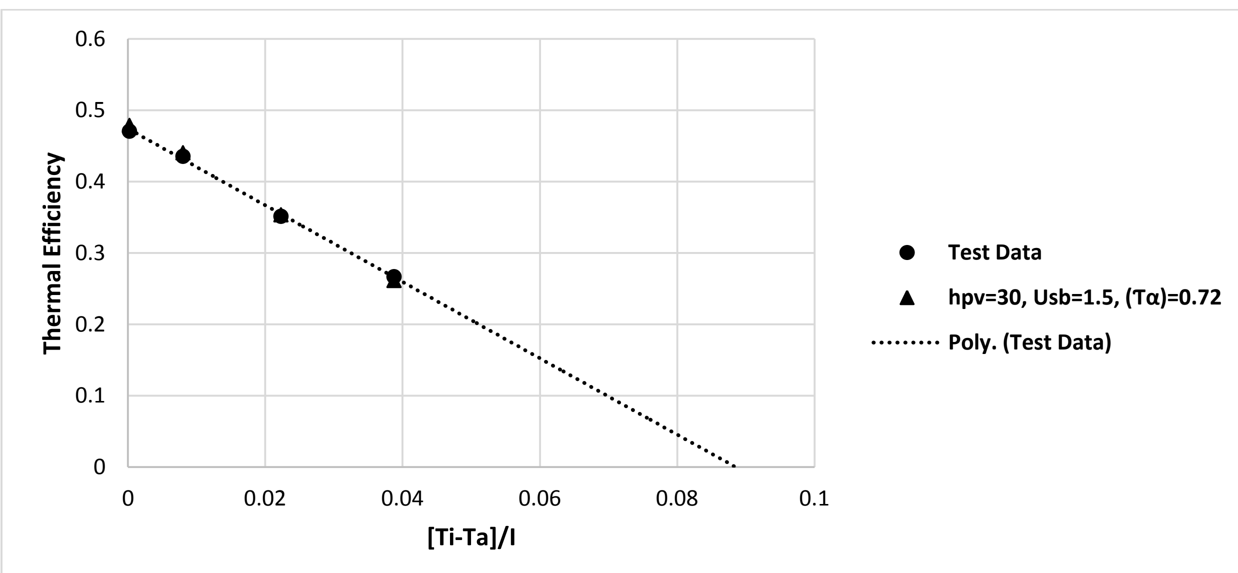

Figure 6: Case B Conditions (mass flow rate = 43 kg/hr, wind speed = 2.6 m/s, PVT On) - Reduced Temperature Thermal Efficiency, Measured vs. Simulated Results

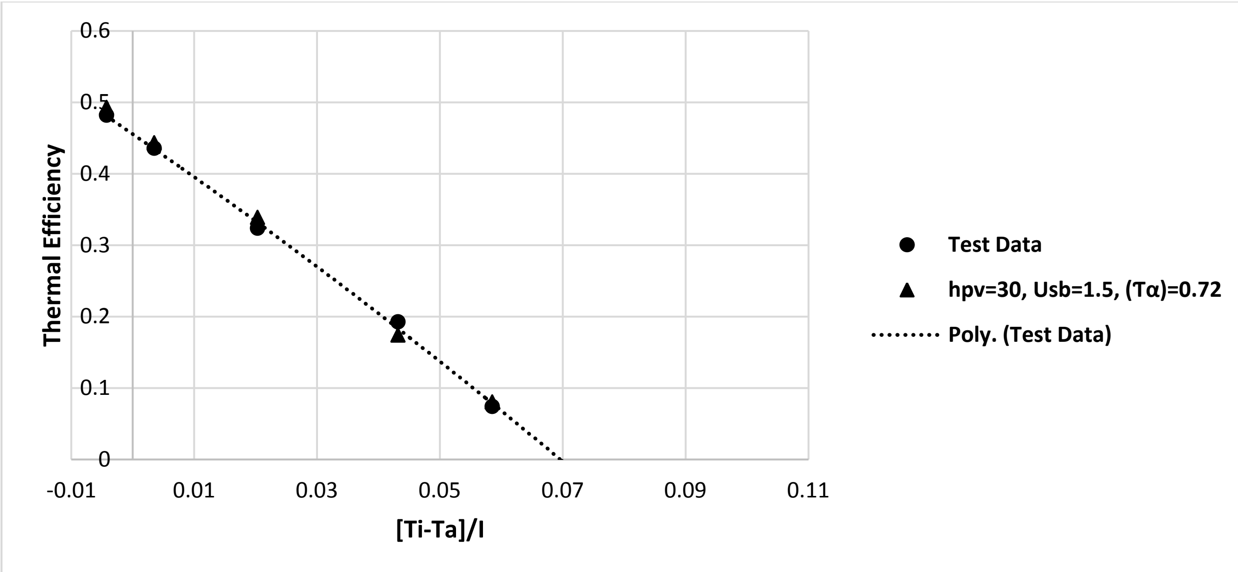

Figure 7: Case C Conditions (mass flow rate = 103 kg/hr, wind speed = 5.8 m/s, PVT On) - Reduced Temperature Thermal Efficiency, Measured vs. Simulated Results

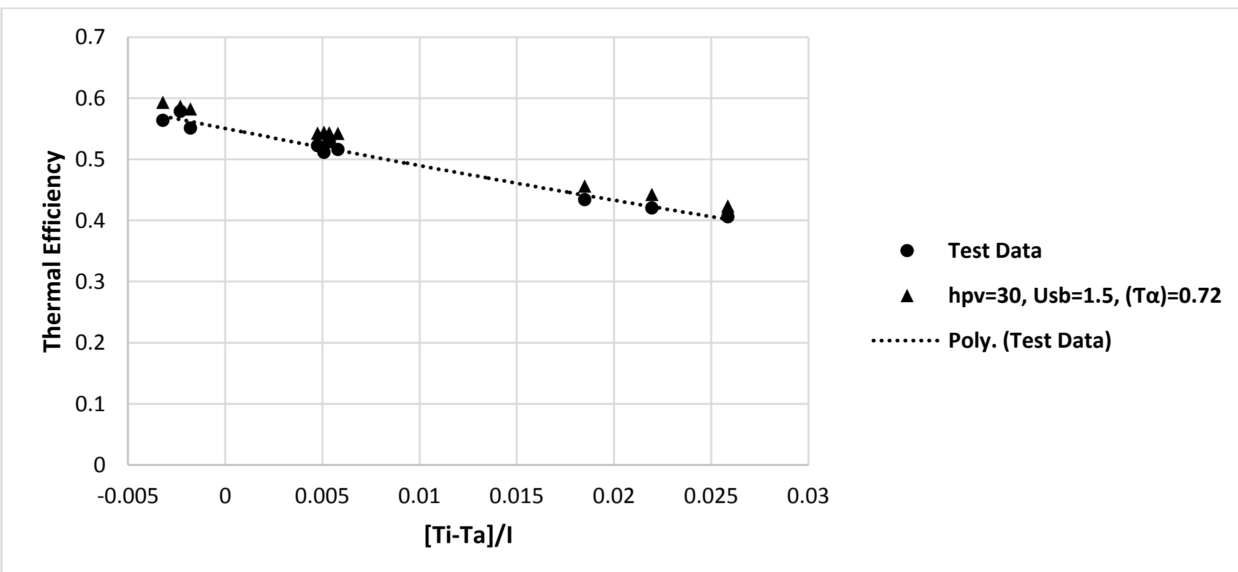

Figure 8: Case D Conditions (mass flow rate = 103 kg/hr, wind speed = 2.6 m/s, PVT Off) - Reduced Temperature Thermal Efficiency, Measured vs. Simulated Results

3.2 System Model Validation

To ensure that the overall system model is accurate, validation was conducted against a TRNSYS (Klein & al., 2017) model. The same simulation input parameters were used in both models, including weather data, panel characteristics, system layout, heat exchanger effectiveness, and building heating loads. The test consisted of a 232.3 m^2 (2500 ft^2) residential home with thermal resistance value (RSI) of 3m^2·K/W] (R-17 ft^2·°F·h/Btu) insulation on the exterior walls, RSI 5.6 (R-32) at the roof, and a basement with RSI 1.6 (R-9) insulation around the perimeter. The home heating load simulation was carried out using e-Quest (DOE, 2016), which generated hourly heating and cooling loads for the building.

Simulations of the solar panel were then carried out using ISO standard testing conditions (ISO, 2013). The fluid input temperatures to the panel that were selected were each measured relative to the ambient temperature, and the following temperature differences were used: -5°C, +5°C, +20°C, +50°C, and +80°C. These conditions were then combined with solar irradiances of 400 W/m^2, 700 W/m^2, and 1000 W/m^2 for each temperature condition, resulting in a total of 15 simulation conditions. It is important to note that these conditions were selected to provide a wide range of operating cases, and that negative thermal efficiencies may occur. In these cases, heat loss through the solar collector would be exhibited, which would correspond to a non-operational state if the system were implemented in a realistic setting. The physical characteristics of the panel are summarized in Table 3.

Table 3: PVT Physical Parameters for System Validation with TRNSYS

Variable	Symbol	Value	Unit
Collector Area	Ac	39.75	m^2
PV Bond Conductance	h_{PV}	100	W/m^2*K
Cover Emissivity	ε_c	0.88	-

Plate Emissivity	ε_p	0.90	-
Pipe-Fluid Heat Transfer Coefficient	h_{fi}	400	W/m^2*K
Pipe Diameter	d	0.01	M
Pipe Spacing	W	0.2	M
Side-Bottom Loss Coefficient	U_{sb}	1.5	W/m^2*K
Absorber Conductivity	k_{abs}	400	W/m*K
PV Conductivity	k_{PV}	84	W/m*K
Absorber Thickness	δ_{abs}	0.0004	m
PV Thickness	δ_{PV}	0.04	m
Collector Tilt	β	45	degrees
Electrical Efficiency at 20oC	η_e	12.44	%
Thermal Efficiency (Zero Loss Collector Efficiency)	η_t	0.6047	-
Efficiency slope	-	0.0004836	%

Using these simulation input parameters, a relationship between the panel reduced temperature and the panel thermal efficiency was generated. The results were then used with the MATLAB *curvefit* tool (MathWorks, 2018), which uses the non-linear least squares fitting procedure, to generate the second-order efficiency correlations for the panel. A plot of the simulation results, with the second-order efficiency correlation, is shown in Figure 9.

The coefficients from these correlations were input into TRNSYS for use with a Type 1a simulation object. A schematic overview of the TRNSYS model is shown in Figure 10. In the TRNSYS system, solar energy was collected using a 39.75 m^2 solar array. The flowrate of fluid in the solar array was controlled with on on-off control scheme, using two differential temperature controllers. The first controller compared the temperature of the fluid exiting the solar array (i.e. Type 1a) with the temperature of the fluid entering on the building heating side of the counterflow heat exchanger (i.e. Type 91). When the temperature of the fluid exiting the solar array was greater than the temperature of the fluid entering the building heating side of the heat exchanger, then this controller was set to “ON”. Similarly, a second controller compared the temperature of the fluid at the outlet and inlet to the solar array, and when the outlet temperature was greater than the inlet temperature this controller was set to “ON”. When both of these controllers output the “ON” signal, the fluid flow rate in the solar array was set to 0.02 kg/s/m2.

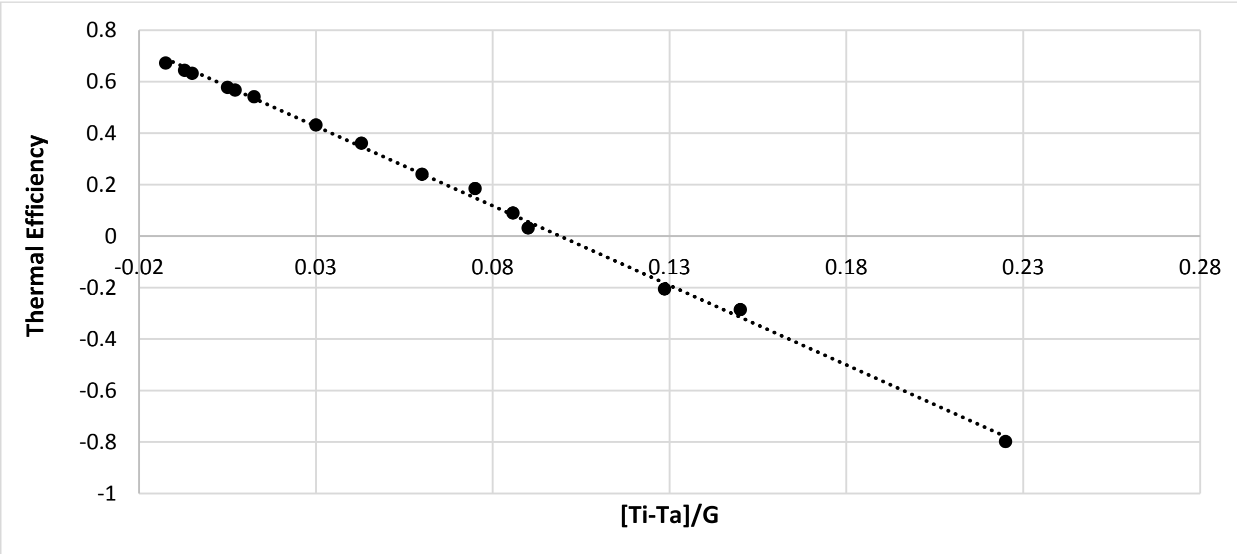

Figure 9: Thermal Performance vs. Reduced Temperature for PVT Panel used in TRNSYS and Custom Model Validation Simulations

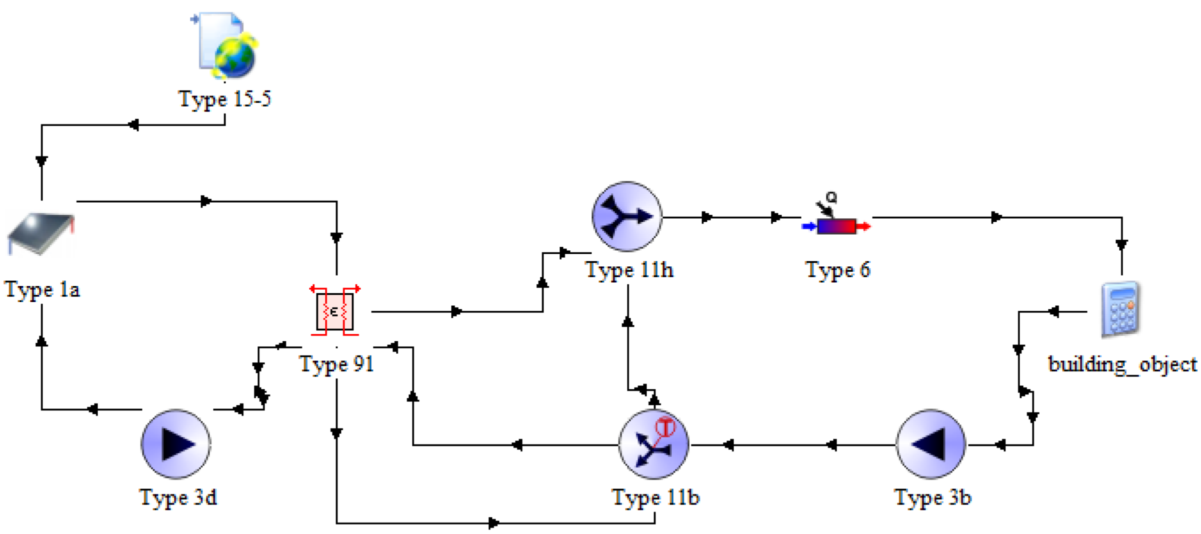

Figure 10: TRNSYS System Layout Schematic

The useful solar heat gain from the PVT array in a time-step was a function of the reduced temperature in that time-step, and the second order thermal efficiency correlation developed for this simulation was used to estimate the thermal energy gain. A counterflow heat exchanger

(TRNSYS Type 91) was used as the heat exchange mechanism between the solar loop and the building space-heating loop. To replicate the setup described in Section 5, a constant supply temperature was ensured by using a recirculation loop for the return loop with a tempering value (i.e. Type 11b) and tee piece (i.e. Type 11h), with an auxiliary heater (Type 6).

Using this system layout, control scheme, and input weather and building load data, the energy outputs from the TRNSYS simulation were compared to the energy outputs from the simulation of the custom system model developed in this paper. The TRNSYS model predicted 7,062 MJ of total useful solar thermal energy gain for the system while the custom model predicted 7,318 MJ. Therefore, the relative energy generation difference between the two models was 3.6%, which was deemed acceptable for this study. For illustrative purposes, the monthly useful solar energy gains for each simulation are shown in Figure 11.

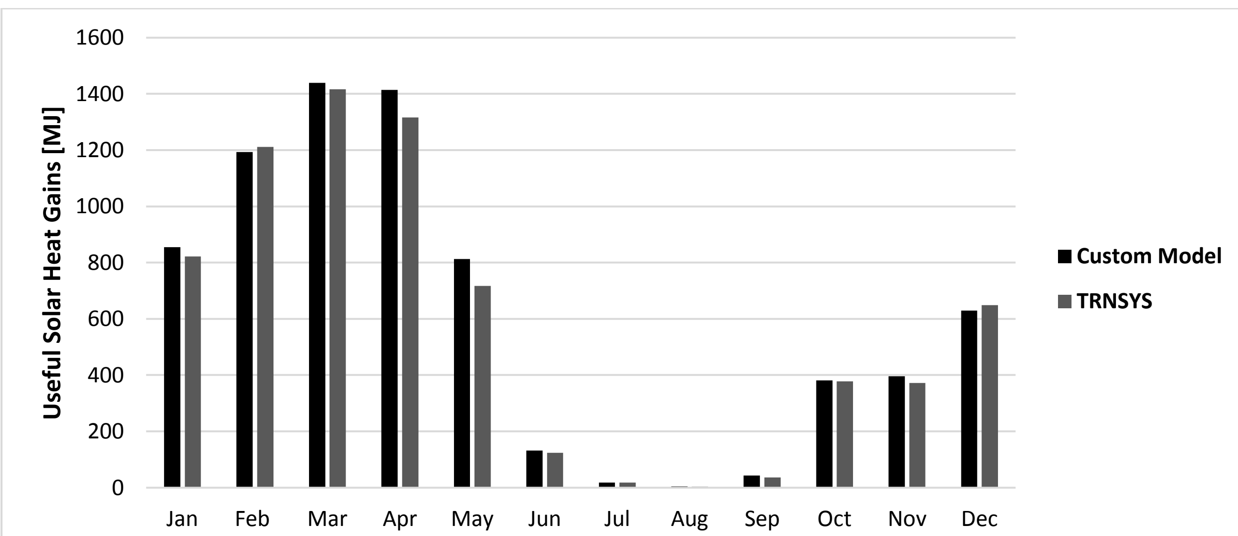

Figure 11: Useful Solar Heat Gain by Month for Custom Model and TRNSYS

4 Results

4.1 Optimal Flow Rate Investigation

An in-depth analysis was performed for several test cases to evaluate the effects of flow rate at different building loads, and heating supply temperatures. The PVT collector array described in Section 3.2, and system set up described in Section 2.2 were used for this analysis. The tests calculate the steady-state conditions of the system at flow rates ranging from 0.04 kg/s to 0.832 kg/s in 0.08 kg/s increments. External conditions for the tests were set to have a wind speed of 5 m/s, solar flux of 2.5 MJ/m^2/hr, and ambient air temperature of 0°C. Ten tests were conducted: two building heating loads of 4 MJ/10 minutes and 8 MJ/10 minutes, each at five different heating supply temperatures ranging from 35°C to 70°C.

It was observed that the optimal flow rate occurs when the heat capacities of the two streams are equal. Figure 12 and Figure 13 each show the results of the five tests cases at a heating load of 4 MJ/10 minutes and 8 MJ/10 minutes respectively. The black line in each figure is the heat capacity of the solar loop, and the coloured solid lines are the heat capacitates of the heating side fluid streams passing through the heat exchanger. At each of their intersections with the black line, the thermal efficiency for that case (represented by the double arrow line) is at its peak. The thermal efficiency then decreases from its maximum point as the flow rate increases.

The loop heat capacity is linearly dependant on the flow rate because the heat capacity of the fluid is assumed constant across all temperatures. The solar loop heat capacity (CP) therefore increases linearly with the flow rate. The heat capacities of the heat exchanger loops are observed to remain constant, except for the two cases where the heating supply temperatures are 35°C and 40°C with a heating load of 4 MJ/10 minutes as seen in Figure 12. In those cases, the solar loop causes the heat exchanger output to the building to increase above the heating supply temperature. Heating return fluid is mixed with the heat exchanger output fluid to reduce its temperature, causing the flow through the heat exchanger to decrease.

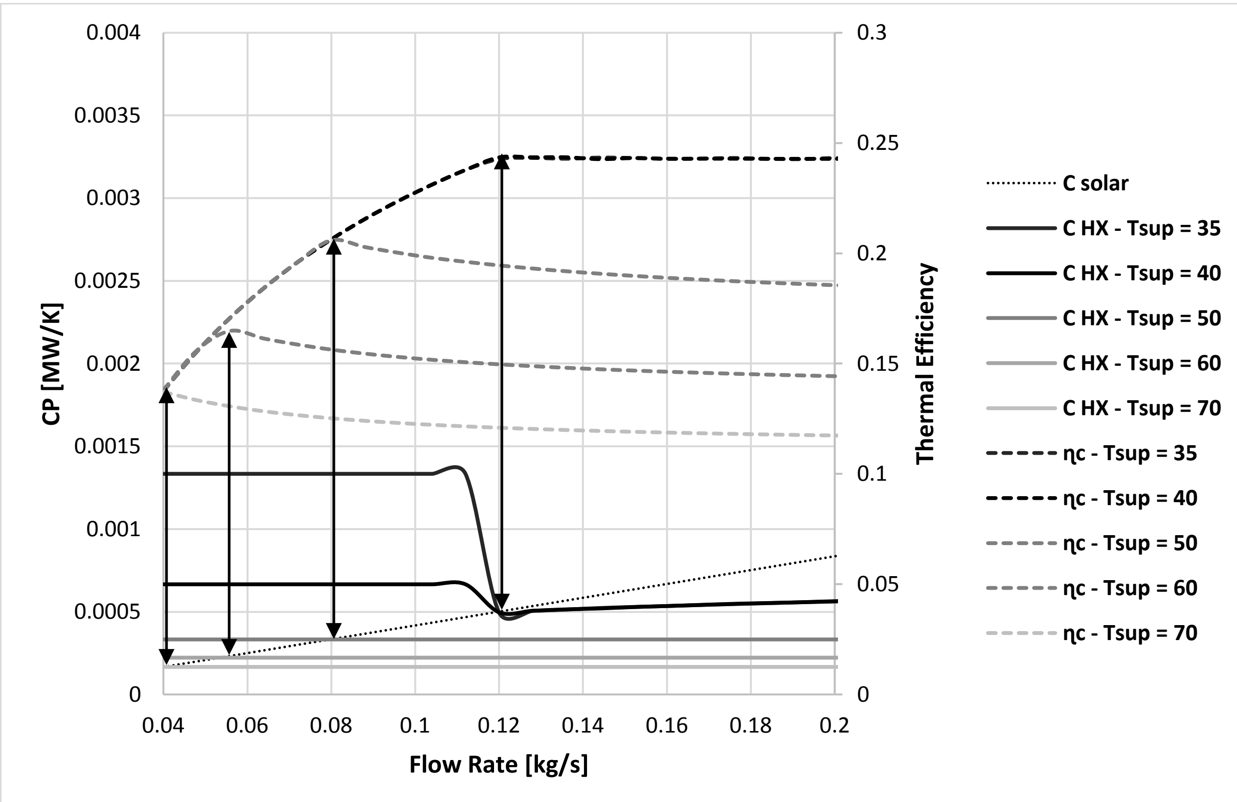

Figure 12: Thermal Efficiency and Loop Heat Capacities vs. Flow Rate; Heating Supply Temperature Ranges from 35°C to 70°C, Heating Load 4 MJ/10 minutes. Vertical Black Double Arrows Indicate the Point of Optimal Thermal Efficiency for Each Heating Supply Temperature

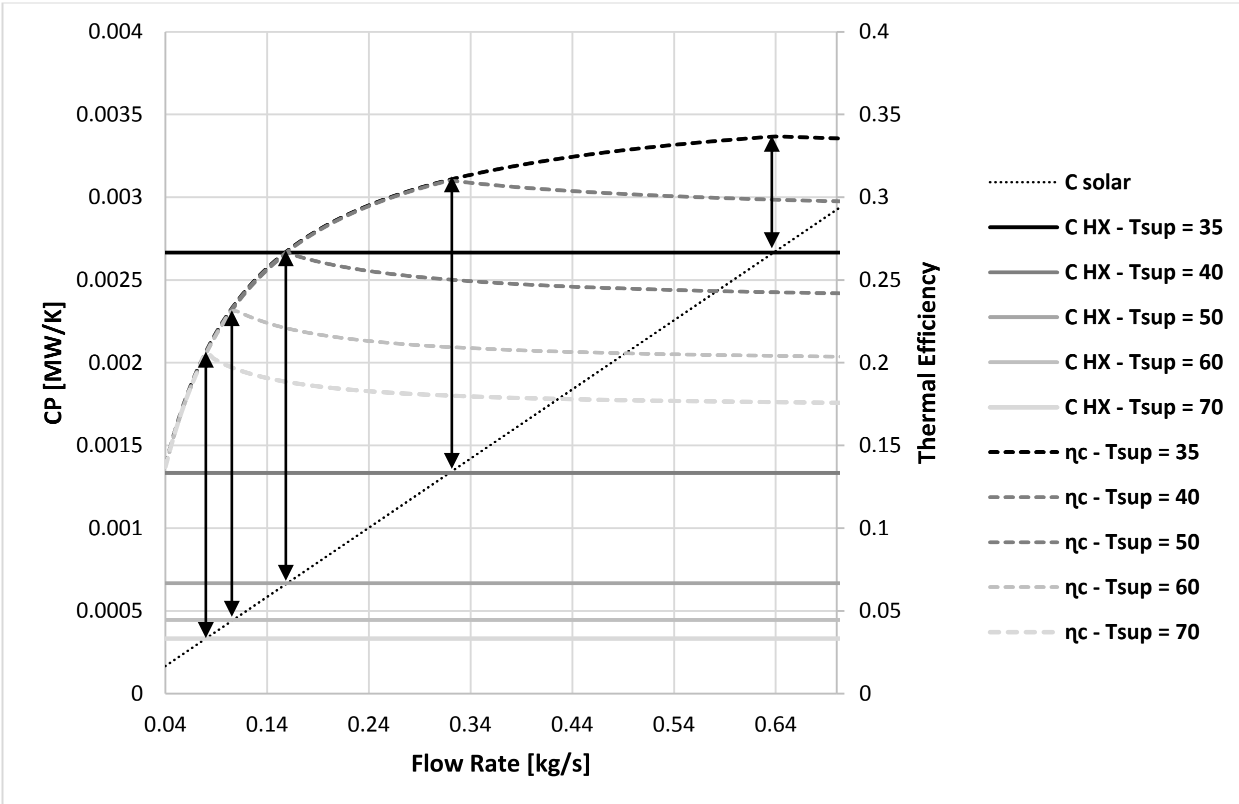

Figure 13: Thermal Efficiency and Loop Heat Capacities vs. Flow Rate. Heating Supply Temperature Ranges from 35°C to 70°C, Heating Load 8 MJ/10 minutes. Vertical Black Double Arrows Indicate the Point of Optimal Thermal Efficiency for Each Heating Supply Temperature

The tests demonstrate that increasing the heating supply temperature will cause the thermal efficiency to peak at a lower solar flow rate, and that the peak is greater than the efficiency plateau that occurs at higher flow rates. Increasing the building heating load results in higher thermal efficiency at all heating supply temperatures. This occurs because as the solar flow rate increases, the entire collector temperature decreases, resulting in less thermal losses to the environment and greater useful heat gains. However, from Eq. (11) the rate of heat transfer is limited to the lesser of the heat capacity of the two streams. When the heat capacity of the heating side loop is greater than the solar loop, all of the solar thermal energy collected can be transferred to it. Once the solar loop surpasses the flow rate of the space-heating loop, C_{min} stops increasing and the amount of useful energy that can be extracted from the collectors becomes fixed. As the solar flow rate is increased beyond the optimal point, the solar outlet temperature begins to decrease. Looking again at Eq. (11), with C_{min} fixed, the rate of heat transfer will decrease linearly with solar outlet temperature. Figure 14 shows the solar inlet and outlet temperatures, and thermal efficiency versus flow rate for the test case with a heating supply temperature of 50°C and building load of 8 MJ/10 minutes. It can be seen that both the inlet and outlet temperatures begin to converge after the optimal point and that the thermal efficiency decreases. A larger heating load requires a greater flow rate for the same temperature difference between the heating supply and return, resulting in a greater minimum possible stream heat capacity (C_{min}).

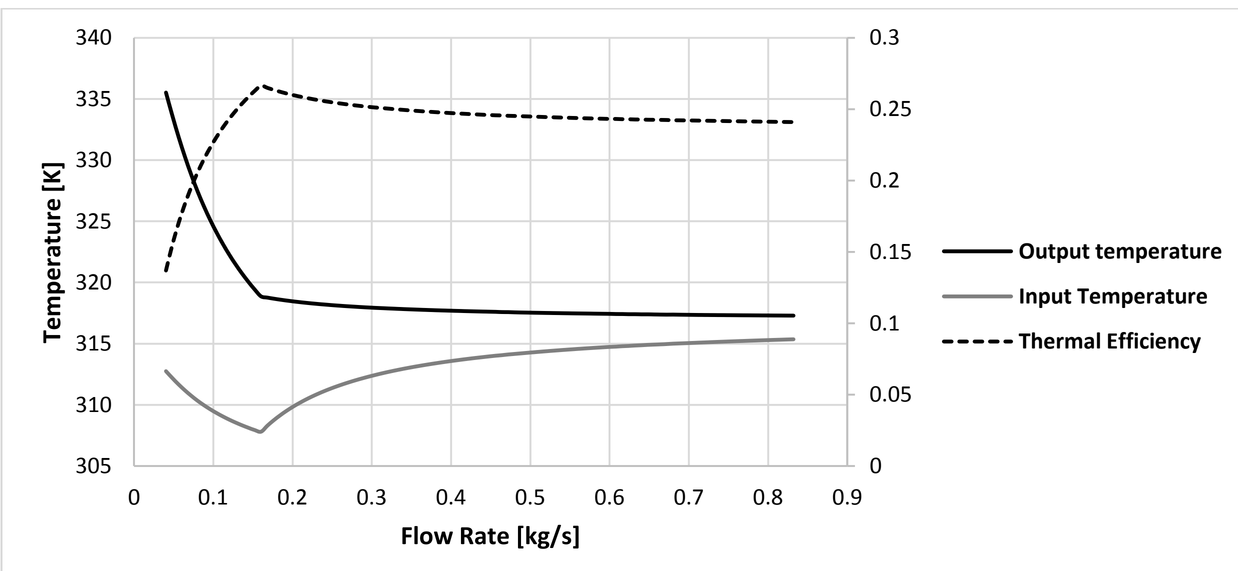

Figure 14: Thermal Efficiency and Collector Input/Output Temperatures vs. Flow Rate. Heating Supply Temperature Ranges from 50°C, Heating Load 8 MJ

4.2 Optimal Flow Rate Simulation

The findings of Section 4.1 concluded that the benefit from a variable flow rate strategy in the system could be seen when the solar loop flow rate matched that of the heating loop passing through the heat exchanger. Simulations were run to quantify said benefits using the sample home, and solar array described in Section 3.2. Heating supply temperature was identified as being a critical parameter to the system benefiting from variable flow, and so two separate values of 35°C and 60°C were tested. For each, a simulation using a constant flow, and variable, optimal flow strategy was conducted.

The results were evaluated using the following metrics: (1) total amount of thermal energy generated while the other system is inoperable; and (2) total amount of thermal energy generated in excess of the other system during timesteps when both are in operation. The combined total of thermal energy produced by the solar array and auxiliary heater were compared to the total building heating load as well to assess the level of accuracy of the simulation. These parameters are summarized in Table 4, and the monthly solar gains for the simulations with heating supply temperatures of 35°C and 60°C can be seen in Figure 15 and Figure 16 respectively.

Table 4: Analysis Metrics for Constant and Optimal Flow Simulations

Flow Strategy	**Useful Solar Thermal Energy [MJ]**	$\sum \boldsymbol{Q_u}$**; total when the other flow strategy is inoperable [MJ]**	$\sum \Delta \boldsymbol{Q_u}$ **; gross advantage when both strategies are operable [MJ]**	$\boldsymbol{Q_u + Q_{aux} - B_{load}}$ **[MJ]**	$\boldsymbol{Q_u + Q_{aux} - B_{load}}$ **[%]**
heating Supply Temperature = 35°C					
Constant	7,317.75	0.02	114.66	114.31	0.13
Optimal	7,407.56	40.76	163.72	0	0
heating Supply Temperature = 60°C					
Constant	4,440.84	1.17	47.13	40.16	0.06
Optimal	4,973.70	0	581.16	0	0

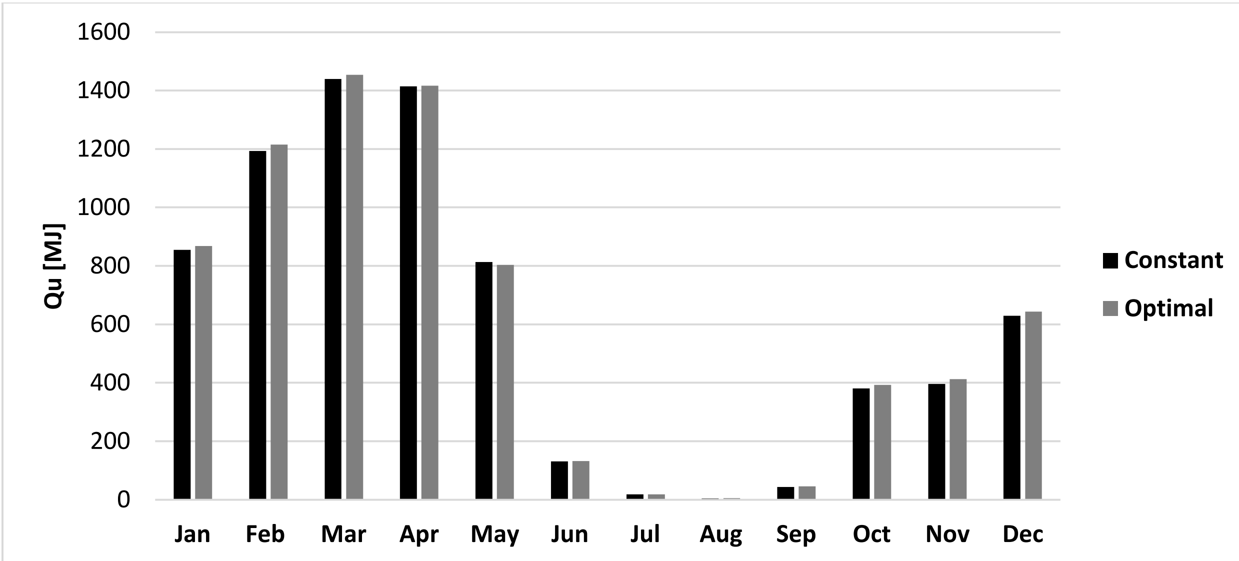

Figure 15: Monthly Useful Solar Heat Gains for Constant vs. Optimal Flow Rate Strategies with Heating Supply Temperature 35°C

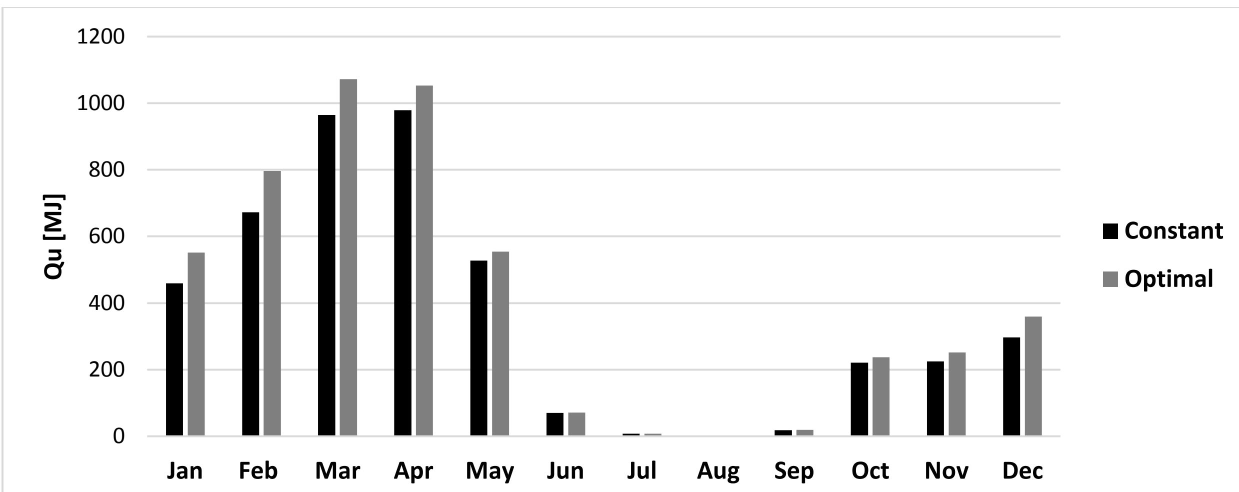

Figure 16: Monthly Useful Solar Heat Gains for Constant vs. Optimal Flow Rate Strategies with Heating Supply Temperature 60°C

The results show that the optimal flow control strategy produced more total useful solar heat gains at both heating supply temperatures. In accordance to the observations made in Section 4.1, the relative benefit of the optimal flow strategy over constant flow is greater when the heating supply and return temperature difference is greater. With a supply temperature of 35°C, the optimal flow simulation produced 1.2% more useful solar heat than the constant flow simulation, while that value increased to 12.0% with a supply temperature of 60°C.

Although the simulation predicts the constant flow rate strategy producing more useful thermal energy than the optimal flow rate strategy during some time steps, it is a result of calculation error rather than an error with the strategy. The iteration convergence values are finite, leading to a small amount of error in each time step. The largest discrepancy between the simulations in a time step when constant flow produced more solar thermal energy was 0.147 MJ. To assess the impact of the iteration convergence values, that particular time step was simulated at flow rates ranging from 0.04 kg/s to 0.8 kg/s (0.08 kg/s intervals). Annual simulation convergence values of 0.01°C for the solar inlet fluid loop, and 0.001 kg/s for the heating side heat exchanger loop were used, and this was then repeated with 0.001°C and 0.0001 kg/s values, respectively. The results are displayed in Figure 17. When the model uses the more stringent convergence values, the useful energy at the nominal flow rate used in the constant flow simulation is reduced from 0.595MJ to 0.456 MJ. Compared to the optimal flow simulation, the difference between the two simulations is reduced from 0.147 MJ to 0.005 MJ.

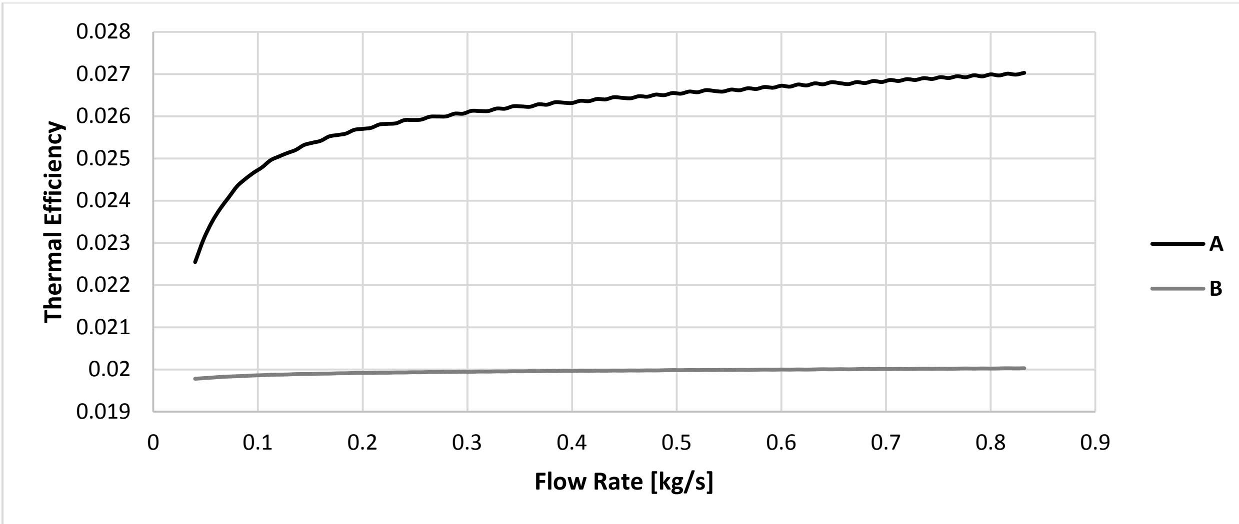

Figure 17: Thermal Efficiency vs. Flow Rate Using Convergence Values Of: 0.01°C and 0.001 kg/s (A), and 0.001°C and 0.0001 kg/s (B)

5 Conclusions

In order to investigate the potential benefits of variable control strategies for PVT collectors, a new steady state modelling technique was developed using a modification of the method given by Duffie and Beckman (Duffie & Beckman, 1991) in which the overall loss coefficient and heat removal factors are updated at each time step. The proposed method allows variations in flow rate to be modelled, improving model accuracy at high reduced temperatures by accounting for changes in wind speed and ambient temperatures. The model was validated using test data for the Volther Powertherm obtained from the solar simulation laboratory at Concordia University.

The PVT model was next simulated in conjunction with a building heating system interfaced with a counterflow heat exchanger. A parallel system was created in TRNSYS in which a sample house was heated by a PVT array and a backup auxiliary heater. A full-year simulation was run to validate the system model with TRNSYS with a useful solar heat gain discrepancy of 3.6% between models.

Ten test cases were simulated using the custom system model with varying heating supply temperatures and building heating loads. The steady state condition of each case was determined for solar loop flow rates ranging from 0.04 kg/s to 0.832 kg/s in 0.08 kg/s increments. Analysis of the results revealed that the optimal operating point for any set of conditions at steady state occurs when the heat capacity rates of the solar loop and building heating loop are equal. It was also found that at higher heating supply temperatures, the overall solar heat gains were reduced, but the relative difference between optimal and nominal flow rates increased. The test case with a 5°C difference between heating supply and return temperatures showed a 0.7% relative increase in thermal efficiency from nominal to optimal flow, and the case with a 30°C difference had a 17.1% increase.

The full system model developed in this paper was then used to conduct a case study for a house comparing a constant nominal flow rate with the optimal flow control strategy. The simulations using the optimal flow strategy predicted a 1.2% increase in useful annual thermal energy gains from the solar array when the building heating loop had a temperature difference between the supply and return of 5°C, and a 12.0% increase when it was 30°C.

To summarize, an optimal variable flow rate strategy for PVTs shows significant potential to increase thermal efficiency in systems using direct transfer from the solar loop to the heating process using a counterflow heat exchanger, and is increasingly effective the larger the temperature difference between the heating supply and return temperatures are. One limitation of this study is that only one building typology, one solar collector type, and a single climate zone have been simulated using the model and optimal flow rate strategy developed in this thesis. Future research to investigate the variable-flow approach using different types and combinations of solar collectors such as selective flat plate and evacuated tubes should be considered, as well as different building types, target processes, and climates. In addition, although the strategy to identify the optimal flowrate has been developed, the corresponding controls strategy has not been implemented and is a topic warranting further investigation, including the financial analysis comparing the cost of implementing flow rate controls with fuel savings associated with the additional thermal energy obtained from the solar thermal system.

Acknowledgements

This research was completed with grant #23575 from the Ontario Centres of Excellence (VIP1) program and Arup Canada Inc. This research was also undertaken, in part, thanks to funding from the Canada Research Chairs program. We would also like to acknowledge the Natural Sciences and Engineering Research Council of Canada, and the Ontario Graduate Scholarship program for funding towards this research.

6 References

Al-Waeli, A. H. et al., 2018. Comparison study of indoor/outdoor experiments of a photovoltaic thermal PV/T system containing SiC nanofluid as a coolant. *Energy,* Volume 151, pp. 33-44.

Al-Waeli, A. H. et al., 2017. Evaluation of the nanofluid and nano-PCM based photovoltaic thermal (PVT) system: An experimental study. *Energy Conversion and Management,* Volume 151, pp. 693-708.

Al-Waeli, A. H., Sopian, K., Kazem, H. A. & Chaichan, M. T., 2017. Photovoltaic/Thermal (PV/T) systems: Status and future prospects. *Renewable and Sustainable Energy Reviews,* Volume 77, pp. 109-130.

Al-Waeli, A. H., Sopian, K., Kazem, H. A. & Chaichan, M. T., 2018. Nanofluid based grid connected PV/T systems in Malaysia: A techno-economical assessment. *Sustainable Energy Technologies and Assessments,* Volume 28, pp. 81-95.

Al-Waeli, A. H. et al., 2018. Comparison of prediction methods of PV/T nanofluid and nano-PCM system using a measured dataset and artificial neural network. *Solar Energy,* Volume 162, pp. 378-396.

Anderson, T., Duke, M., Morrison, G. & Carson, J., 2008. Performance of a building integrated photovoltaic/thermal (BIPVT) solar collector. *Solar Energy,* Volume 83, pp. 445-455.

Badescu, V., 2008. Optimal control of flow in solar collector systems with fully mixed water storage tanks. *Energy Conservation and Management,* Volume 49, pp. 169-184.

Ben cheikh el hocine, H. et al., 2015. Model Validation of an Empirical Photovoltaic Thermal (PV/T) Collector. *Energy Procedia,* Issue 74, pp. 1090-1099.

Calise, F., d'Accadia, M. D. & Vanoli, L., 2012. Design and dynamic simulation of a novel solar trigeneration system based on hybrid photovoltaic/thermal collectors (PVT). *Energy Conversion and Management,* Issue 60, p. 214–225.

Chow, T., 2003. Performance analysis of photovoltaic-thermal collector by explicit dynamic model. *Solar Energy,* Volume 75, pp. 143-152.

DOE, 2016. *eQUEST: the QUick Energy Simulation Tool.* [Online]
Available at: http://www.doe2.com/equest/

Dubey, S., Sarvaiya, J. & Seshadri, B., 2013. Temperature dependent photovoltaic (PV) efficiency and its effect on PV production in the world–a review. *Energy Procedia,* Volume 33, pp. 311-321.

Dubey, S. & Tiwari, G. N., 2008. Thermal modeling of a combined system of photovoltaic thermal (PV/T) solar water heater. *Solar Energy,* Volume 82, pp. 602-612.

Duffie, J. & Beckman, W., 1991. In: *Solar Engineering of Thermal Processes.* 2nd ed. New York: John Willey and Sons Inc., pp. 777, 250-326.

H, A.-W. A., T, C. M., K, S. & A, K. H., 2017. Energy Storage: CFD Modeling of Thermal Energy Storage for a Phase Change Materials (PCM) added to a PV/T using nanofluid as a coolant. *Journal of Scientific and Engineering Research,* 4(12), pp. 193-202.

Hollands, K. & Brunger, A., 1992. Optimum flow rates in solar water heating systems with a counterflow heat exchanger. *Solar Energy,* 48(1), pp. 15-19.

ISO, 2013. *ISO/FDIS 9806:2013(E): Solar energy — Solar thermal collectors — Test methods.* Geneva: International Organization for Standardization.

Kalogirou, S. A., 2001. Use of TRNSYS for modelling and simulation of a hybrid pv–thermal solar system for Cyprus. *Renewable Energy,* Volume 23, pp. 247-260.

Klein, S. & al., e., 2017. *TRNSYS 18: A Transient System Simulation Program.* Madison: Solar Energy Laboratory, University of Wisconsin.

Krauter, S. C. W., 2006. *Solar Electric Power Generation - Photovoltaic Energy Systems.* Berlin, Heidelberg: Springer.

Kumar, A., Baredar, P. & Qureshi, U., 2015. Historical and recent development of photovoltaic thermal (PVT) technologies. *Renewable and Sustainable Energy Reviews,* Volume 42, pp. 1428-1436.

MathWorks, 2018. *MATLAB Curve Fitting Toolbox Help Page.* [Online] Available at: https://www.mathworks.com/help/curvefit/custom-nonlinear-models.html

Nasrin, R., Hasanuzzaman, M. & Rahim, N., 2018. Effect of high irradiation and cooling on power, energy and performance of a PVT system. *Renewable Energy*, 116(A), pp. 552-569.

Nhut, L. M. & Park, Y. C., 2013. A study on automatic optimal operation of a pump for solar domestic hot water system. *Solar Energy,* Volume 98, pp. 448-457.

Nualboonrueng, T., Tuenpus, P., Ued, Y. & Akisawa, A., 2013. The performance of PV-t systems for residential application in Bangkok. *Progress in Photovoltaics*, Volume 21, pp. 1204-1213.

Sathe, T. M. & Dhoble, A., 2017. A review on recent advancements in photovoltaic thermal techniques. *Renewable and Sustainable Energy Reviews*, Volume 76, pp. 645-672.

Solimpeks, 2016. *Powertherm.* [Online] Available at: http://www.solimpeks.com/product/volther-powertherm/ [Accessed 16 01 2019].

Touafek, K., Haddadi, M. & Malek, A., 2011. Modeling and Experimental Validation of a New Hybrid Photovoltaic Thermal Collector. *IEEE Transactions on Energy Conversion,* Volume 26.

TRNSYS, 2018. *TRNSYS Mathmatical References,* Madison: University of Wisconsin.

Vokas, G., Christandonis, N. & Skittides, F., 2005. Hybrid photovoltaic–thermal systems for domestic heating and cooling—A theoretical approach. *Solar Energy,* Issue 80, pp. 607-615.

Yazdanifard, F., Ebrahimnia-Bajestan, E. & Ameri, M., 2016. Investigating the performance of a water-based photovoltaic/thermal (PV/T) collector in laminar and turbulent flow regime. *Renewable Energy,* Volume 99, pp. 295-306.

Zondag, H. A., De Vries, D. W., Van Helden, W. G. J. & Van Zolingen, R. J. C., 2001. The Thermal and Electrical Yield of a PV-Thermal Collector. *Solar Energy*, Volume 72, pp. 113-128.